Comparision of neoclassical rotation theory with experiment under a variety of conditions in DIII-D

W. M. Stacey and J. Mandrekas
Fusion Research Center, Georgia Institute of Technology, Atlanta, Georgia 30332

A neoclassical theory of gyroviscous radial momentum transport and poloidal and toroidal rotation has been compared with experiment in DIII-D [Luxon, Anderson, Batty *et al.*, *Plasma Physics and Controlled Nuclear Fusion Research 1986* (IAEA, Vienna, 1987), Vol. 1, p. 159] discharges in different confinement regimes, with a range of neutral beam powers and with co- and counter-injection, and with various types of dominant impurity species present. Calculated central toroidal rotation velocities and momentum confinement times agreed with experiment over a wide range of these conditions, with one notable exception in which a drift correction may be needed to reduce the gyroviscous toroidal force. Radial distributions of toroidal and poloidal rotation velocities and radial electric field, calculated using the radial distribution of toroidal angular momentum input density, agreed with measured distributions for the one time in an L-mode discharge that was examined in detail. © *2002 American Institute of Physics.*
[DOI: 10.1063/1.1464892]

I. INTRODUCTION

A self-contained set of coupled models for the calculation of plasma toroidal and poloidal rotation velocities, poloidal density asymmetries, the radial electric field, and neoclassical particle and momentum transport in tokamak plasmas has recently been assembled.[1] Prior to implementing this set of models in a transport code, which would allow the self-consistent calculation of plasma density, temperature and rotation profiles, we have used experimental density, temperature, and normalized toroidal rotation profiles to calculate certain other rotation parameters that depend both on these profiles and on the theoretical model.

We recently found agreement between the predicted and measured central rotation velocities and momentum confinement times in a series of three L-mode (low confinement mode) shots with different neon concentrations and in one H-mode (high confinement mode) shot in DIII-D.[2] The first purpose of this paper was to extend this type of theory/experiment comparison of central rotation velocities and momentum confinement times for DIII-D shots in other confinement regimes [quiescent H-mode (QH), quiescent double barrier (QDB), internal transport barrier (ITB)], with high-Z (nickel and copper) and low-Z (carbon) dominant impurities, and with co- and counter-injected neutral beams.

The comparison described in the previous paragraph provides an integral check of the theory against experiment, i.e., a comparison of momentum confinement times and of the magnitude of a fixed velocity profile. A more comprehensive comparison of the theory with experiment for the calculation of radial profiles of toroidal and poloidal velocities and the radial electric field is the second purpose of this paper.

After briefly describing the gyroviscous theory of momentum transport in Sec. II, we compare in Sec. III predicted central rotation velocities and momentum confinement times with experimental values. In Sec. IV, we compare the predicted toroidal and poloidal rotation velocities and radial electric field radial distributions with measured values in a DIII-D L-mode shot. These results are summarized in Sec. V, where conclusions are presented.

II. GYROVISCOSITY

Radial momentum transport in tokamaks is widely regarded as being anomalous. However, it was shown[3] some time ago that Braginskii's gyroviscous theory[4] when extended to toroidal geometry[5] could predict the momentum confinement times in a number of shots in seven different tokamaks spanning a wide range of physics and machine parameters. More recently, it was shown[2] that this same theory, when extended to include also the calculation of toroidal rotation and a convective contribution to the momentum confinement time,[1] agreed with the measured momentum confinement times and central rotation velocities in one co-injected H-mode (high) DIII-D discharge with a large carbon impurity content and in three co-injected L-mode (low) DIII-D discharges with varying amounts of injected neon.

Braginskii[4] [and others (e.g., Refs. 6 and 7)] derived the viscous stress tensor for charged particles in a magnetic field using the general rate-of-strain tensor of fluid theory. He found three structurally different components of the viscous stress tensor associated with "parallel," "perpendicular," and "gyro" viscosity. Stacey and Sigmar[5] and Mikhailovskii and Tsypin[7] subsequently extended the Braginskii gyroviscous stress tensor to toroidal geometry, and the latter authors introduced a drift correction.

In computing the flux surface average of the toroidal component of the viscous force, which determines the cross-field transport of toroidal angular momentum, the "parallel" component vanishes identically and the "perpendicular" component has a coefficient which is about four orders of magnitude $(1/\Omega\tau)$ smaller than the gyroviscous coefficient, where Ω is the gyrofrequency and τ is the collision time. (It is the smallness of this "perpendicular" viscosity coefficient

Phys. Plasmas, Vol. 9, No. 5, May 2002

Comparision of neoclassical rotation theory . . .   1623

that has led to the belief that viscosity is anomalous.) The gyroviscous component of the toroidal viscous force in toroidal geometry is[5]

$$\langle R^2 \nabla \phi \cdot \nabla \cdot \pi_{34} \rangle = \left\langle \frac{1}{R h_p} \frac{\partial}{\partial l_\psi} \left(R^3 h_p \eta_4 \frac{\partial (V_\phi R^{-1})}{\partial l_p} \right) \right\rangle$$

$$= \frac{1}{2} \Theta G \frac{nmT}{eB} \frac{V_\phi}{R} + O(\varepsilon^3)$$

$$\equiv R_0 mn V_\phi \nu_d, \tag{1}$$

where

$$G \equiv -\frac{r}{\eta_4 V_\phi} \frac{\partial}{\partial r} (\eta_4 V_\phi) = r(L_n^{-1} + L_T^{-1} + L_{V_\phi}^{-1}), \tag{2}$$

and where h_x and dl_x are the metric and length elements in the x-direction (i.e., $dl_x = h_x dx$), $\eta_4 = nmT/eB$ is the gyroviscosity coefficient, $L_x^{-1} = -(dx/dr)/x$ is the inverse radial gradient scale length, the subscripts ψ and p refer to the "radial" and "poloidal" directions, and the other symbols are common usage (R = major radius, V_ϕ = toroidal velocity, n = density, T = temperature, m = mass, B = magnetic field, e = unit charge, r = radial variable). Flux surface geometry has been replaced by toroidal geometry, a Fourier expansion of the poloidal dependencies of the form $x(r,\theta) = x^0(r)(1 + x^c \cos\theta + x^s \sin\theta)$ has been made, and a poloidal asymmetry factor has been defined

$$\Theta = \left[4 + \left(\frac{n^c}{\varepsilon} \right) \right] \left(\frac{V_\phi^s}{\varepsilon} \right) + \left[1 - \left(\frac{V_\phi^c}{\varepsilon} \right) \right] \left(\frac{n^s}{\varepsilon} \right)$$

$$= \left[4 + \left(\frac{n^c}{\varepsilon} \right) \right] \left\{ - \left(\frac{B_\phi}{B_\theta} \frac{V_\theta}{V_\phi} \right) \left[\left(\frac{\Phi^s}{\varepsilon} \right) + \left(\frac{n^s}{\varepsilon} \right) \right] + \left(\frac{\Phi^s}{\varepsilon} \right) \right\}$$

$$+ \left(\frac{n^s}{\varepsilon} \right) \left\{ \left(\frac{B_\phi}{B_\theta} \frac{V_\theta}{V_\phi} \right) \left[2 + \left(\frac{\Phi^c}{\varepsilon} \right) + \left(\frac{n^c}{\varepsilon} \right) \right] - \left(\frac{\Phi^c}{\varepsilon} \right) \right\}, \tag{3}$$

where Φ indicates the electrostatic potential and B_θ is the poloidal magnetic field. For simplicity, the species subscript has been suppressed in Eqs. (1)–(3). The second form of Eq. (3) results from using the radial component of the momentum balance equation to express the toroidal velocity in terms of other variables. Equation (1) defines the angular momentum radial transport, or "drag," frequency ν_d.

We solved numerically the moments (1, $\sin\theta$, $\cos\theta$) of the poloidal momentum balance equations for a 2-species (ion-impurity) model [Eqs. (15)–(17) of Ref. 8, Eqs. (9)–

(11) of Ref. 1] to obtain the poloidal velocities and the sin and cos components of the density, then used the poloidal component of the electron momentum balance equation to relate the poloidal components of the electrostatic potential to the poloidal components of the ion and impurity densities.

III. COMPARISON OF THEORY AND EXPERIMENT: CENTRAL ROTATION VELOCITIES AND MOMENTUM CONFINEMENT TIMES

We compared predicted and measured momentum confinement times and central toroidal rotation speeds in a number of different types of DIII-D discharges.

Since the calculated toroidal rotation velocities for different ion species are usually about the same and only the impurity rotation velocity can be measured, an approximate calculation of the toroidal rotation velocity can be made from an overall angular momentum balance on the plasma,

$$\Gamma_\phi \equiv \sqrt{\frac{2m_b}{E_b}} P_b R_{\tan}$$

$$= \frac{(2\pi R) \int_0^a \langle R \Sigma_j^{\text{ions}} n_j m_j V_{\phi j} \rangle 2\pi r dr}{\tau_\phi^{\text{th}}}$$

$$= \frac{V_{\phi 0}(2\pi R) \Sigma_j^{\text{ions}} \int_0^a \langle R n_j m_j f_v \rangle 2\pi r dr}{\tau_\phi^{\text{th}}}, \tag{4}$$

where Γ_ϕ is the beam (subscript b) torque input, $R_{\tan}$ is the average tangency radius of the beamlines, and τ_ϕ^{th} is the "theoretical" momentum confinement time defined below from the gyroviscous theory.

In the last form of Eq. (4), we have written the toroidal rotation velocity as the product of a central value and a radial profile function, $V_\phi(r) = V_{\phi 0} f_v(r)$. We use this second form and the theoretical momentum confinement time of Eq. (5) to calculate the theoretical value of $V_{\phi 0}$. We do not presently have the capability to calculate the normalized velocity profile function $f_v(r)$, so we use $f_v(r)$ [and $n_j(r) = n_0 f_n(r)$] from experiment. Using the known input beam torque and the theoretical angular momentum confinement time, a value of $V_{\phi 0}^{\text{th}}$ then can be calculated for comparison with experiment.

The theoretical angular momentum confinement time is defined as the total angular momentum content of the plasma divided by the integrated radial angular momentum transport rate by gyroviscosity plus convection,

$$\tau_\phi^{\text{th}} = \frac{(2\pi R) \Sigma_j^{\text{ions}} \int_0^a \langle R n_j m_j V_{\phi j} \rangle 2\pi r dr}{2\pi R \Sigma_j^{\text{ions}} [\int_0^a \langle R^2 \nabla \phi \cdot \nabla \cdot \pi_{34} \rangle 2\pi r dr + \int_0^a \langle R \nabla \cdot (n_j m_j V_{\phi j} V_{rj} \hat{e}_r) \rangle 2\pi r dr]}. \tag{5}$$

Note that density and toroidal velocity radial distributions appear both in the numerator and denominator of Eq. (5). Thus, writing $V_\phi(r) = V_{\phi 0} f_v(r)$ and $n(r) = n_0 f_n(r)$, the n_0 and $V_{\phi 0}$ cancel out, and only the normalized profile func-

tions (f_n and f_v) are needed from experiment. However, both T_0 and $f_T(r)$ must be taken from experiment (or otherwise calculated).

In summary, the normalized profile functions (f_n, f_T,

TABLE I. Comparison of predicted and measured toroidal rotation speeds and momentum confinement times in DIII-D.

Shot time	Mode, NBI, impurity	P_{nbi} MW	$\bar{n}$ 10^{19} m^{-3}	T_{i0}/T_{e0} keV	$V_{\varphi 0} \div V_{thD}$	τ_φ^{th} ms	τ_φ^{exp} ms	$V_{\varphi 0}^{th}$ 10^5 m/s	$V_{\varphi 0}^{exp}$ 10^5 m/s
98777 1.6 s	L, Co Carbon	4.5	3.42	3.5/2.5	0.31	80	73	1.52	1.50
98775 1.6 s	L, Co Neon	"	4.05	6.3/3.3	0.37	147	152	2.90	3.06
99411 1.8 s	H, Co Carbon	9.2	4.80	8.3/3.9	0.32	93	84	2.90	2.64
106919 2.0 s	QH, Ctr Ni–Cu,	9.32	2.58	10.9/3.9	0.40	44	45	3.86	3.98
106919 3.5 s	"	"	2.83	14.2/4.2	0.38	64	68	4.21	4.48
106956 3.1 s	QDB Ctr CuNi,	11.77	3.75	15.1/4.4	0.24	44	46	2.41	2.51
102942 0.85 s	H, Co Carbon	4.89	2.36	1.8/2.5	0.40	55	51	2.20	2.02
102942 1.25 s	ITB, Co carbon	7.08	2.67	4.8/4.2	0.35	52	72	2.94	4.01

f_v) and the amplitude T_0 were taken from experiment to evaluate the theoretical momentum confinement time of Eq. (5), and the profile functions (f_n, f_v) and amplitude n_0 were then also taken from experiment to solve Eq. (4) for $V_{\phi 0}^{th}$. Even though the experimental value of the normalized profile factor f_v is used, this procedure provides a discriminating test of the theoretical model for π_{34}, because if we were to use a different model for π_{34} and carry through the same calculation we would get a different answer for $V_{\phi 0}^{th}$ and τ_ϕ^{th}. For example, if we carry through exactly the same calculation using the experimental profile f_v but using the neoclassical perpendicular viscosity, which differs from the first form of Eq. (1) by the replacement of η_4 with $\eta_2 = \eta_4/\Omega\tau$ and the replacement of the poloidal l_p derivative with a radial l_ψ derivative,[5] we obtain a value for τ_ϕ^{th} that is two orders of magnitude larger than shown in Table I for the calculated and measured confinement times.

We calculated the radial momentum flux from an extended neoclassical transport theory[1] in which the particle flux appearing in Eq. (5), $\Gamma_{rj} = n_j V_{rj}$, consists of (1) the Pfirsch–Schlüter flux of Hinton–Hazeltine;[9] (2) the banana-plateau flux of Stacey et al.[10] supplemented by the thermal friction contribution of Hinton–Hazeltine;[9] (3) the direct beam-ion momentum exchange flux of Ohkawa;[11] (4) the inertial flux of Burrell–Ohkawa–Wong;[12] and (5) the radial electric field driven flux of Stacey et al.[10] The form of the flows used in evaluating these fluxes included the effects of parallel and gyroviscous momentum transport.[10]

We note that viscosity and convection can only transport momentum from the center to the edge of the plasma, where other processes (e.g., charge exchange, magnetic field ripples) transfer it from the edge of the plasma to the wall or magnets. We assume that the time required for transfer of angular momentum from the center to the edge of the plasma dominates the overall angular momentum removal rate. Thus, we compare Eq. (5) for the theoretical momentum confinement time with a definition of the "experimental" confinement time as the ratio of total angular momentum content of the plasma to the total input torque,

$$\tau_\phi^{exp} = \frac{2\pi R \Sigma_j^{ions} \int_0^a \langle R n_j m_j V_{\phi j}\rangle 2\pi r\, dr}{\Gamma_\phi}. \tag{6}$$

We use experimental values for $n(r) = n_0 f_n(r)$ and for $V_\phi = V_{\phi 0} f_v(r)$ to evaluate Eq. (6).

To facilitate the numerical evaluation of the integrals appearing in the above expressions, we make a few approximations. The term in square brackets in Eq. (1) is evaluated by calculating both the poloidal asymmetry factor of Eq. (3) and the radial convective flux at the half radius ($\rho = \frac{1}{2}$). The radial profile functions $f_{n,v,T}$ were fit numerically to the experimental data using a profile form of a parabola raised to a power sitting on a pedestal. The pedestal values were taken directly from experiment, and the powers were determined numerically. We employed the same numerical approximations to evaluate the integrals in Eqs. (5) and (6).

The central rotation speed was measured directly (or at least it could be constructed by extrapolating measured data inward). The "experimental" momentum confinement time was constructed by using the measured rotation profiles to evaluate the integral in Eq. (6), using the same numerical approximations described in the previous paragraph for the evaluation of the integrals in the theoretical quantities.

The results of the theory/experiment comparison are shown in Table I; calculated and measured central rotation velocities are compared in the last two columns, and calculated and measured momentum confinement times are compared in the preceding two columns. These results are discussed below.

A. L-mode shots 98777 and 98775 (Refs. 13 and 14)

Two co-injected L-mode shots which were operated identically in every respect except for the injection of neon were previously analyzed[2] but are included here for completeness. There was agreement between predicted and measured values of momentum confinement times and central rotation speeds, and of the difference in these quantities due

to the neon injection. Although the convective contribution to the calculated momentum confinement time was negligible in the no-neon shot, the increase in the theoretical confinement time with the injection of 2.8% neon concentration was due entirely to an increase in the predicted inward convective momentum flux. In these shots at $\rho = \frac{1}{2}$, the calculated in–out (cosine component) and up–down (sine component) density asymmetries were $O(10^{-2}\varepsilon)$ and $O(10^{-4}\varepsilon - 10^{-3}\varepsilon)$ for deuterium and $O(10^{-1}\varepsilon)$ and $O(10^{-2}\varepsilon)$ for carbon.

B. H-mode shot 99411 (Ref. 15)

A high performance ($H_{89} = 3.0$) co-injected H-mode shot with a relatively high (5%) carbon impurity content was also previously analyzed[2] and is included for completeness. Again, there was agreement between predicted and experimental central rotation speeds and momentum confinement times. The calculated deuterium cosine and sine components were $O(10^{-2}\varepsilon)$ and $O(10^{-3}\varepsilon)$, and the calculated carbon cosine and sine components were $O(10^{-1}\varepsilon)$ and $O(10^{-2}\varepsilon)$. The calculated inward convective contribution to the momentum confinement time was about 15%.

C. Quiescent mode shots 106919 and 106956 (Ref. 16)

Two counter-injected QH-mode (quiescent high) shots with relatively low plasma densities and large nickel and copper concentrations were analyzed. The predicted momentum confinement times and central rotation speeds were in agreement with experiment.

In the QH-mode shot 106919, the impurity concentration built up continuously over the discharge (Z_{eff} at $\rho = \frac{1}{2}$ increased from 4.10 at 2010 ms to 5.43 at 3510 ms), consistent with an increasing inward convective momentum flux which contributed about 10% to the predicted momentum confinement time at 2010 ms, but which contributed about 35% at 3510 ms. The predicted cosine and sine components at $\rho = \frac{1}{2}$ at 3510 ms were $O(10^{-2}\varepsilon)$ and $O(10^{-4}\varepsilon)$ for deuterium plus carbon "main ion" species, and were $O(10^{-1}\varepsilon)$ and $O(10^{-2}\varepsilon)$ for the nickel plus copper "impurity" species in the 2-species model calculation.

In the QDB-mode shot 106956, an increase in beam power during the discharge produced a sharp gradient in the density (but not the temperature) profile inside of $\rho = \frac{1}{2}$, which is indicative of an internal transport barrier. The calculated poloidal asymmetries in density were similar to those given in the previous paragraph, and the convective contribution to the momentum confinement time was about 5%.

D. H-mode shot 102942 with internal transport barrier (Ref. 17)

In co-injected H-mode shot 102942, the measured temperature and toroidal velocity profiles were more sharply peaked, throughout the discharge, than in the other shots examined. The density profile was flat early in the shot, but sharp density and electron temperature gradients developed inside of $\rho = 0.25$ later in the shot following an increase in beam power, indicating the formation of an internal transport barrier.

We compared the predicted and measured rotation speeds before (850 ms) and after (1250 ms) the formation of the internal transport barrier (ITB). The agreement was good before the formation of the internal transport barrier, but rather poor after the formation of the ITB. The toroidal viscous force of Eq. (1) overpredicted radial transport of toroidal moment after formation of the ITB, as reflected in a significant under-prediction of the momentum confinement time and the central rotation speed.[17]

The predicted cosine and sine components of the density asymmetry at $\rho = \frac{1}{2}$ at 850 ms were $O(10^{-2}\varepsilon)$ and $O(10^{-3}\varepsilon)$ for deuterium and $O(10^{-1}\varepsilon)$ and $O(10^{-2}\varepsilon)$ for carbon. The calculated convective contribution to the momentum confinement time was about 10%.

E. Mikhailovskii–Tsypin drift correction

We believe that this disagreement after ITB formation may be explained by the Mikhailovskii–Tsypin drift correction[7] to the Braginskii gyroviscous stress tensor, on which Eq. (1) is based. Claassen et al.[18] have shown that this correction is negligible when $\xi \equiv (\rho_{\theta i}/L_{pi})/(V_{\phi i}/V_{thi}) \ll 1$, which is the usual situation in the interior of a strongly rotating tokamak plasma. However, the combination of a strongly peaked ion temperature profile and the steep gradient in the density at the internal transport barrier just inside of $\rho = 0.25$ makes this parameter take on a maximum value of $\xi \approx 1.5$ at that location at 1250 ms. Thus, the gyroviscous toroidal force of Eq. (1) would be expected to be reduced inside of $\rho = 0.25$ by the Mikhailovskii–Tsypin drift correction. Claassen et al.[18] estimated an order of magnitude reduction when $\xi \approx O(1)$, but we would expect somewhat less of a reduction because ξ is only $O(1)$ over a small part of the plasma. We found that it was necessary to reduce the toroidal viscous force of Eq. (1) by a factor of 4 to obtain agreement with experiment at 1250 ms. By comparison, the maximum value of the parameter $\xi \approx \frac{1}{2}$ just inside of $\rho = 0.25$ in this shot at 850 ms, before the formation of the internal transport barrier.

In the other shots considered in this paper, which had either relatively flat density profiles or only moderately peaked ion temperature profiles, or both, the maximum value of the parameter was $\xi < 1$ throughout the core plasma and the average value was $\xi \ll 1$. Of course, ξ became large in the plasma edge, where the rotation speed was small and the ion pressure gradient scale length became smaller than in the center. However, other momentum transfer processes (e.g., charge exchange, magnetic field ripple) dominated in the edge plasma in any case, and it was the time required to transport momentum from the center to the edge that determined the overall momentum confinement time.

IV. COMPARISON OF THEORY AND EXPERIMENT: RADIAL PROFILES OF TOROIDAL AND POLOIDAL VELOCITY AND RADIAL ELECTRIC FIELD

A more direct comparison of theory and experiment was achieved by calculating the radial distribution of rotation ve-

locities and radial electric field. An expression for the flux surface averaged impurity toroidal rotation velocity on a given flux surface (normalized radial location ρ) was derived[10] by using the perpendicular and flux surface aver-

aged parallel components of the momentum balance equation and the form of the poloidal velocity $V_\theta = KB_\theta/n$ that resulted from solving the particle balance equation to obtain an expression for the impurity (I) rotation velocity,

$$V_{\phi I} = \frac{\left\{ [\hat{M}_{\|_i} + (1+\xi_i)\hat{M}_{\|_I}] - [\hat{\mu}_I(1+\xi_i)P_I' + \hat{\mu}_i P_i'] + [\hat{\mu}_I(1+\xi_i) + \hat{\mu}_i]\left(\dfrac{E_r}{B_\theta}\right) \right\}}{\xi_i(1+\xi_I) + \xi_I} \tag{7}$$

and a similar expression for the main ion (i) rotation velocity, where the $\hat{\mu}$'s are normalized parallel viscosity terms, the P''s are normalized pressure gradient terms, the $\hat{M}_\|$'s are normalized parallel momentum density input rates from the beams [see Eq. (15) in Ref. 1], and $\xi_j = \hat{\mu}_j + \beta_j$, where β_j is the normalized gyroviscous "drag" term given by

$$\beta_j \equiv \frac{\nu_{dj}}{\nu_{jk}} \tag{8}$$

with ν_{dj} given by Eq. (1).

The flux surface averaged radial electric field at a given ρ-location was obtained by summing the flux surface averaged toroidal momentum balances over species. For an ion-impurity (i,I) model this may be written,[10]

$$\frac{E_r}{B_\theta} = \frac{\{[\hat{\mu}_i + \hat{\mu}_I(1+\xi_i)]\hat{M}_{\phi I} + [\hat{\mu}_I + \hat{\mu}_i(1+\xi_I)]\hat{M}_{\phi i} + [\beta_i + \beta_I(1+\xi_i)]\hat{\mu}_I P_I' + [\beta_I + \beta_i(1+\xi_I)]\hat{\mu}_i P_i'\}}{\hat{\mu}_i[\beta_I + \beta_i(1+\xi_I)] + \hat{\mu}_I[\beta_i + \beta_I(1+\xi_i)]}. \tag{9}$$

In order to evaluate the ν_d terms from Eq. (1), it was necessary to solve Eq. (7) and the three (1, sine, cosine) moments of the poloidal momentum balance equations[8] [to obtain the Θ terms of Eq. (3)], and to solve Eq. (9) for the radial electric field, all at each radial location. In addition, we used the experimental ion temperature and the experimental profiles of density, ion temperature and toroidal velocity (to calculate L_n, L_T, $L_{V\phi}$) to evaluate the ν_d terms from Eq. (1).

The beam momentum density input rate was calculated using our neutral beam deposition and fast ion slowing down code NBEAMS.[19] This code has been successfully benchmarked against the Monte Carlo neutral beam deposition code NFREYA.[20]

The predicted values of the toroidal angular velocity and radial electric field are compared with the measured angular velocity and radial electric field (which is constructed from fits to the measured rotation velocity and pressure gradients) in Figs. 1 and 2 for the co-injected L-mode shot 98777 at 1600 ms. [This shot was selected because the convective momentum transport (which we can not yet treat in the calculation of radial distributions) is small,[2] and this time was chosen because the data have been extensively analyzed.] The curves labeled $\Theta_{cal}G(L_{exp})$ indicate that the results were calculated with Θ and G evaluated as described above. These calculations were in rather good agreement with experiment; the maximum error in the calculated rotation velocity was less than 15%.

The predicted poloidal velocities [calculated with Eqs. (9)–(12) of Ref. 1] for carbon and deuterium and the "measured" poloidal velocity for carbon are shown in Fig. 3. The "measured" poloidal velocity is actually constructed from a measurement of the velocity along a line-of-sight, and the

uncertainty in the poloidal velocity is comparable to its magnitude.[21]

Any approximation errors in the calculation of poloidal velocities and density asymmetries and experimental errors enter our model through the product ΘG in Eq. (1). The factor Θ is calculated for analytic toroidal geometry with circular cross sections, using a low order Fourier expansion. The factor G depends on the ion pressure and toroidal velocity gradient scale lengths, which we construct by differentiating the corresponding experimental profiles. In order to test the sensitivity of these results to possible uncertainties in the data and in the numerical procedures, we made a second set
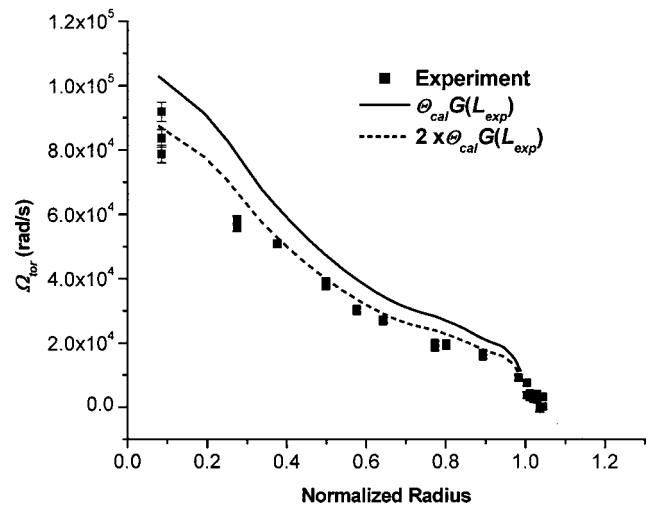

FIG. 1. Comparison of the calculated toroidal angular velocity Ω_ϕ with experiment for different values of the product ΘG (DIII-D shot 98777 at 1.6 s).
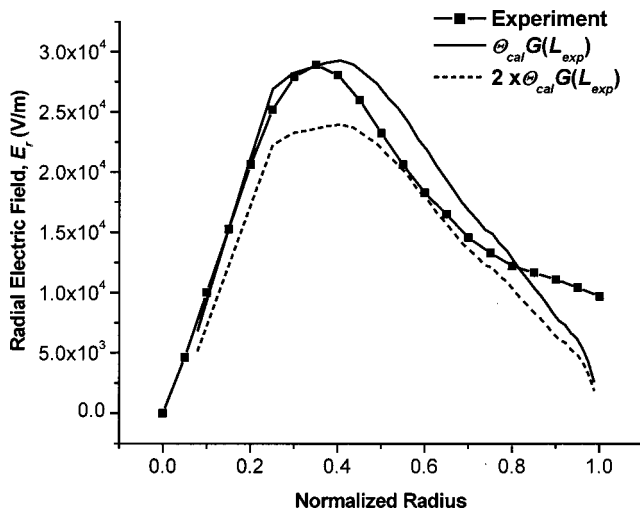
FIG. 2. Comparison of the calculated radial electric field E_r with experiment for different values of the product ΘG (DIII-D shot 98777 at 1.6 s).

of calculations in which the product ΘG is multiplied by a factor of 2. As shown in Figs. 1 and 2, the results are relatively insensitive to this change.

To further test the sensitivity of our simulations to the details of the momentum input rate distribution, our simulations were repeated using the input torque profile calculated by the TRANSP code[22] for this shot. For $\rho \leq 0.8$, the fast ion deposition profile calculated with TRANSP agrees with the one obtained with the NBEAMS code, and thus the calculated toroidal velocity and radial electric field profiles were quite similar to those shown in Figs. 1 and 2, for both values of the product ΘG. However, the TRANSP torque profile becomes negative for $\rho \geq 0.8$, probably due to the treatment of fast ion first orbit losses and the associated $J \times B$ torque.[22] Since our model does not include these fast ion loss and $J \times B$ effects, we can not use the TRANSP torque for $\rho \geq 0.8$ in our calculation.

It should be noted here that the profile calculation presented in this section does not include convective momentum transport effects. Such effects were estimated to be small in
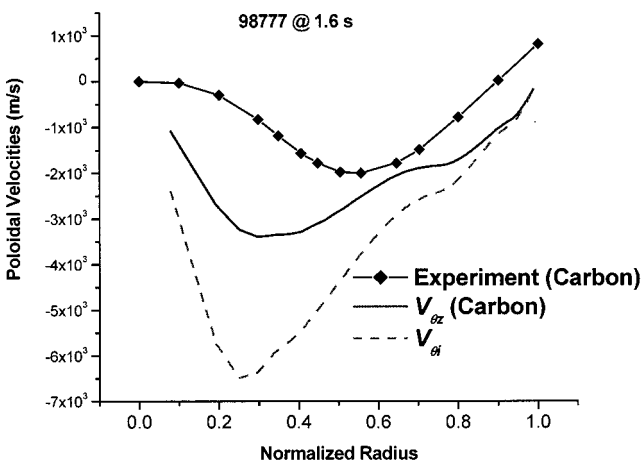
this shot, using the methods described in the previous section. In a full transport calculation, the radial particle flux would be calculated and used directly in the calculation of the rotation velocity from the toroidal momentum balance equation.

V. SUMMARY AND CONCLUSIONS

A neoclassical rotation theory, based on gyroviscous radial transport of toroidal angular momentum, was compared with experiments in DIII-D. Using experimental values for the normalized radial profiles of density, temperature, and toroidal rotation velocity and using experimental values for the central density and ion temperature as input, the calculated momentum confinement times and central rotation velocities agreed with experiment for a set of shots in different confinement regimes, with co- and counter-injected neutral beams, and with different dominant impurity species. The one exception was in a shot with an internal transport barrier co-located with a peaked ion temperature profile in which a drift correction omitted from the present gyroviscous model would be expected to be important.

The calculated radial profiles of toroidal and poloidal rotation velocities and radial electric field agreed with experiment (to within $<15\%$ for the toroidal rotation velocity) at the one time in one L-mode shot that was considered in detail. Further comparison of radial profiles in a range of shots will be the subject of a future paper.

These results lead us to conclude that the rotation theory summarized in Ref. 1, which is based on gyroviscous angular momentum transport, can predict the momentum confinement times and toroidal rotation velocities measured in DIII-D under a range of operating conditions. However, inclusion of a drift correction to the gyroviscous force may be necessary to deal with internal transport barriers.

FIG. 3. Comparision of the calculated poloidal velocities with experiment (DIII-D shot 98777 at 1.6 s).

[1] W. M. Stacey, Phys. Plasmas **8**, 158 (2001).
[2] W. M. Stacey and M. Murakami, Phys. Plasmas **8**, 4450 (2001).
[3] W. M. Stacey and D. R. Jackson, Phys. Fluids B **5**, 1828 (1993).
[4] S. I. Braginskii, Rev. Plasma Phys. **1**, 205 (1965).
[5] W. M. Stacey and D. J. Sigmar, Phys. Fluids **28**, 2800 (1985).
[6] A. N. Kaufmann, Phys. Fluids **3**, 610 (1960).
[7] A. B. Mikhailovskii and V. S. Tsypin, Sov. J. Plasma Phys. **10**, 51 (1984).
[8] W. M. Stacey, Phys. Fluids B **4**, 3302 (1992).
[9] F. L. Hinton and R. D. Hazeltine, Rev. Mod. Phys. **48**, 239 (1976).
[10] W. M. Stacey, A. W. Bailey, D. J. Sigmar, and K. C. Shaing, Nucl. Fusion **25**, 463 (1985).
[11] T. Ohkawa and Kaku Yugo Kenkyu, Bessatsu **32**, 1 (1974).

[12] K. H. Burrell, T. Ohkawa, and S. K. Wong, Phys. Rev. Lett. **47**, 511 (1981).

[13] G. R. McKee, M. Murakami, J. A. Boedo *et al.*, Phys. Plasmas **7**, 1870 (2000).

[14] M. Murakami, G. R. Mckee, G. L. Jackson *et al.*, Nucl. Fusion **41**, 317 (2001).

[15] M. Murakami, H. E. St. John, T. A. Caspar *et al.*, Nucl. Fusion **40**, 1257 (2000).

[16] W. P. West, M. R. Wade, C. M. Greenfield *et al.*, Phys. Plasmas **9**, 1970 (2002).

[17] E. J. Doyle *et al.*, Nucl. Fusion (to be published).

[18] H. A. Claassen, H. Gerhauser, A. Rogister, and C. Yarim, Phys. Plasmas **7**, 3699 (2000).

[19] J. Mandrekas, ''Physics models and user's guide for the neutral beam module of the supercode,'' Georgia Tech Fusion Report No. GTFR-102, 1992, available from the National Technical Information Service, NTIS, PB93-121887INZ.

[20] R. H. Fowler, J. A. Holmes, and J. A. Rome, ''NEFREYA: A Monte Carlo beam deposition code for noncircular tokamak plasmas,'' Oak Ridge National Laboratory Report No. ORNL/TM-6845, 1979.

[21] K. H. Burrell, General Atomics (private communication, 2001).

[22] R. J. Goldston, ''Topics in confinement analysis of tokamaks with auxiliary heating,'' in *Basic Physical Processes of Toroidal Fusion Plasmas* (Commission of the European Communities and Monotypia Frachi Citta di Castello, Italy, 1985), Vol. 1, EUR 10418 EN.